Quantification of airflow in the sinuses following functional endoscopic sinus surgery*

Joey Siu[1], Jingliang Dong[2], Kiao Inthavong[2], Yidan Shang[2], Richard George Douglas[1]

[1] Department of Surgery, The University of Auckland, Auckland, New Zealand

[2] School of Engineering, RMIT University, Melbourne, Australia

Rhinology 58: 3, 257 - 265, 2020

https://doi.org/10.4193/Rhin19.387

***Received for publication:**

October 29, 2019

Accepted: January 10, 2020

Abstract

Background: Despite functional endoscopic sinus surgery (FESS) being the standard of care in medically recalcitrant chronic rhinosinusitis (CRS), its effect on sinus ventilation has not been fully characterized. Airflow simulations can help improve our understanding of how surgical strategies affect post-surgical sinus ventilation.

Methods: Eight postoperative sinonasal cavity models were reconstructed from a wide spectrum of CRS patients who had undergone FESS. Computational fluid dynamics modeling of steady-state, laminar, inspiratory airflow was performed. Ventilation was quantified and observed for all the sinuses in each model.

Results: Sinus aeration was enhanced following FESS, particularly in the maxillary and ethmoid sinuses. The degree of improvement was related to the extent of surgery performed. This finding was accentuated at a higher inhalational flow rate of 15L/min. The relationship between ostium size and corresponding sinus inflow was stronger for the maxillary and sphenoid sinuses. Maxillary inflow reached 50% in a mega-antrostomy patient, while negligible flow occurred in the frontal sinuses for except one whom had undergone a modified Lothrop procedure.

Conclusions: This study has quantified sinus airflow in the largest set of post-FESS patients to date, to show that with increasing extensive surgery, the sinus and nasal cavity become more interconnected and functionally interdependent. Accordingly, sinus ventilation is improved. This may have important consequences for pre- and post-surgical assessment and planning, and on predicting how drug delivery treatments and devices can be designed to target the postoperative sinuses.

Key words: chronic rhinosinusitis, computational fluid dynamics, computer simulation, FESS, nasal airflow, nasal cavity, paranasal sinuses, sinusitis

Introduction

Despite functional endoscopic sinus surgery (FESS) being the standard of care in medically recalcitrant chronic rhinosinusitis (CRS), current understanding of the post-FESS sinonasal cavity geometry and ventilation remains limited. In FESS, the goals are to open the obstructed sinus openings (ostia), to improve sinus ventilation and restore mucociliary clearance. While surgery alters anatomy, it does not directly address the inflamed mucosa that is not removed during surgery. Without long term topical postoperative medical management, patients may require revision surgery more frequently[(1)]. Post-FESS patients have significantly altered anatomy and simulating airflow will improve our understanding of how surgical strategies affect post-surgical sinus ventilation, as well as help optimize drug delivery treatments and devices to deliver medication to the sinuses. Although routine medical management of CRS in post-FESS patients relies on topical steroid treatment it is unclear how efficiently topical drugs reach the sinonasal mucosa. Studies of preoperative and healthy models suggested that sinus inflow before surgery is negligible [(2-9)]. A small number of computational fluid dynamics (CFD) studies have evaluated airflow and droplet distribution in post-endoscopic sinus surgery models,

Table 1. Patient demographics and surgical intervention.

Patient	Ethnicity	Gender	Age	Sinonasal or airways disease	Surgery	Models (n=8)	Imaging modality	Timing of scan since surgery (months)	Regular intranasal postoperative medications
1	South African	F	31	CRSsNP	Limited FESS: mini-MMA, partial ethmoid.	A	CT	>36	INCS, saline lavage
					Rev. comp. FESS, maxillary megaantros.	B	CT	17	
2	New Zealand European	F	66	CRSwNP Bronchiectasis	Limited FESS: wide MMA, partial ethmoid.	C	CT	>36	INCS, saline lavage
					Rev. comp. FESS, maxillary megaantros.	D	CT	20	INCS, saline and xylitol lavage
3	New Zealand European	F	60	CRSwNP	Comp. FESS	E	MRI	9	INCS, saline lavage
4	Indian	F	44	CRSwNP Asthma	Comp. FESS	F	MRI	6	INCS, saline lavage
5	Tongan	F	31	CRSwNP	Comp. FESS	G	MRI	6	INCS, saline lavage
6	New Zealand European	M	27	CRS secondary to cystic fibrosis	Multiple previous FESS, MELP, maxillary megaantros.	H	MRI	4	INCS; saline and xylitol rinses, hypertonic nebulized saline, nebulized dornase alpha

Comprehensive FESS = wide MMA (Type II Simmens classification), frontal sinus dissection via agger nasi cells, ethmoidectomy and wide sphenoidectomy. Mini-MMA = miniature middle meatal antrostomy by partial uncinectomy; partial ethmoid. = partial ethmoidectomy; rev. comp. FESS = revision comprehensive functional endoscopic sinus surgery; megaantros. = megaantrostomy; MELP = modified endoscopic Lothrop procedure; CRSwNP = CRS with polyps; CRSsNP = CRS without polyps; INCS = intranasal corticosteroids.

and these suggest that the exchange of air between the nasal passages and sinuses is significantly altered following surgery [2,3,6,10,11]. An unsteady flow simulation was performed on 2 postoperative patients, one of whom had a standard FESS procedure, and the other a modified endoscopic Lothrop procedure (MELP) [10]. All paranasal sinuses were included in these models. Airflow velocity at the maxillary ostia was found to be much greater during inspiration in both subjects. The MELP patient also had significantly increased airflow at the frontal ostium. The increase in airflow velocity was mainly attributed to the larger size of the respective ostia after surgery.

In this study, we used CFD techniques to investigate airflow in 8 postoperative sinonasal cavity models from 6 post-FESS patients. This is the largest series to date studying airflow in the entire post-operative sinonasal cavity.

Material and methods

Patients

Six patients with CRS who had bilateral FESS performed were included in this study (Table 1). Eight postoperative sinonasal cavity models were reconstructed for CFD modeling from either CT scans or MRI scans of these patients which were obtained retrospectively. MRI images were acquired according to a high-resolution imaging protocol [12]. Patients underwent scans more than four months from their last surgery.

Patients 1 and 2 had a bilateral limited FESS as their primary operation. This consisted of a middle meatal antrostomy by partial uncinectomy (Type I Simmens classification) [13] with partial ethmoidectomy in patient 1 and wide middle meatal antrostomy (MMA; Type II Simmens classification) with partial ethmoidectomy in patient 2. They subsequently required revision surgery with a bilateral comprehensive FESS (frontal sinus dissection via agger nasi cells, ethmoidectomy, and wide sphenoidectomy) with maxillary mega antrostomy (Type III Simmens classification) due to persisting disease on clinical follow-up and CT scan. Following revision surgery, each of these patients underwent another postoperative CT scan in the follow-up phase. At this time, they had negligible persisting sinonasal inflammation on endoscopy and scan. Two geometries were created for both patients 1 and 2: i) post-limited FESS ii) post-revision comprehensive FESS and maxillary mega-antrostomy.

Patients 3, 4 and 5 underwent a standard bilateral comprehensive FESS. This consisted of a wide MMA (Type II Simmens classification), frontal sinus dissection via agger nasi cells, ethmoidectomy and wide sphenoidectomy. Patient 6 had a background of cystic fibrosis, and had undergone multiple operations for CRS, the most extensive being a modified endoscopic Lothrop procedure (MELP) and maxillary megaantrostomy in addition to a standard comprehensive FESS. Patients 3 to 6 had fully recovered, with negligible persisting sinonasal inflammation on

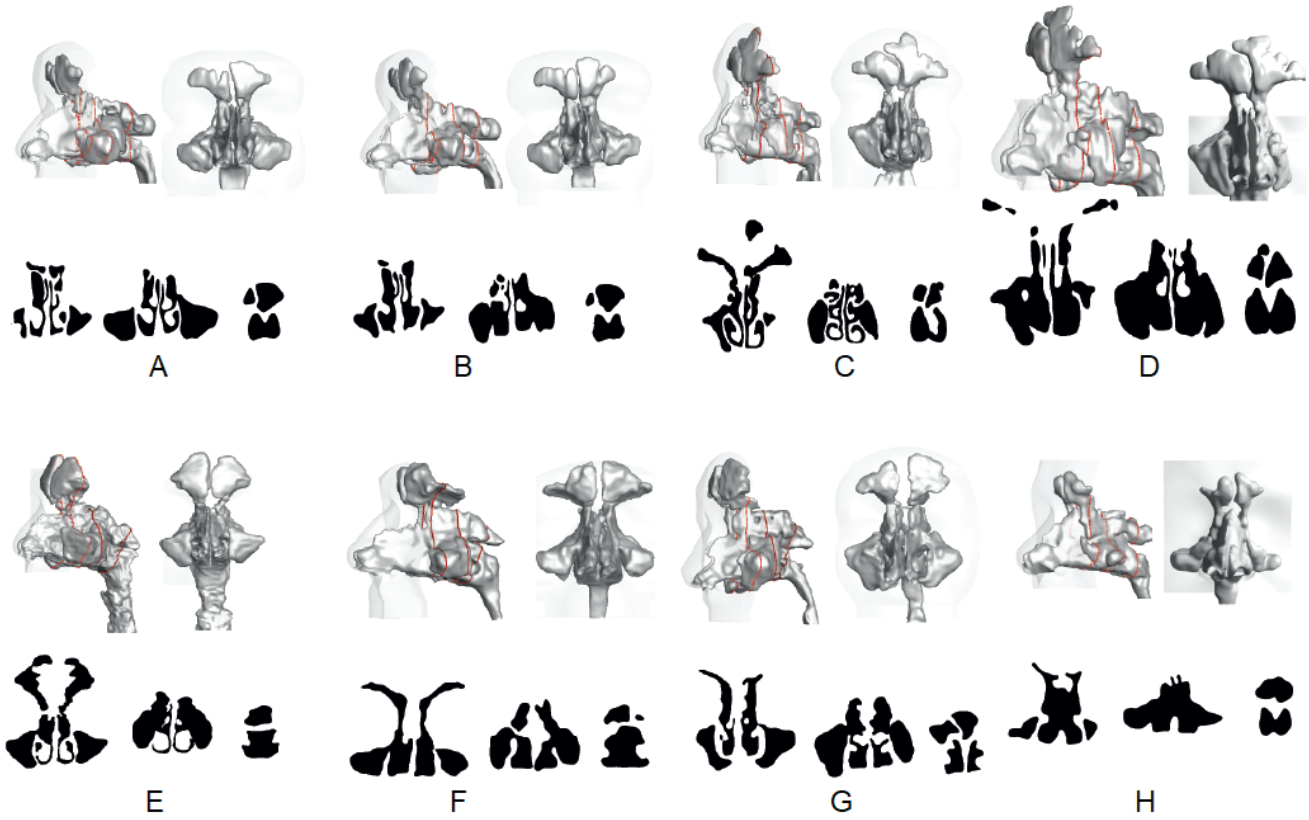

Figure 1. 3D nasal cavity geometry for patients in the study with accompanying selected coronal sections.

endoscopy at the time of their scan.

It was elected not to administer a nasal decongestant to ensure the closest correlation between clinical and radiological assessment and to reflect the most common state of breathing that patients experience in daily life.

Written informed consent was obtained from all patients, and the study was approved by the New Zealand Health and Disability Ethics Committee.

Sinonasal model reconstruction

The scanned images were imported into a medical imaging software package, 3D Slicer® (BWH, MA, USA). After airway segmentation, smoothing and correction for artifacts, a three-dimensional surface geometry of each patient's sinonasal airways, including the outer nose and face was created [14]. Each sinonasal cavity was separated into the following regions: septum, vestibule, main nasal passage (nasal valve to nasopharynx), frontal sinus, maxillary sinus, ethmoid sinus, sphenoid sinus and nasopharynx.

The 3D model was meshed with polyhedral cells with prism layers using ANSYS-Fluent®-ver.19.2 (ANSYS Inc., PA, USA).

The mesh quality was improved by moving nodes so that the maximum skewness in all models were less than 0.65. A mesh independence test was performed by comparing the velocity magnitude on six 2D-cross-sectional planes15 of one model and the minimum mesh cell size for the optimum mesh was adopted across all models. This resulted in all models with optimized mesh between 1.5-2.2 million poly-hexcore and prism cells. Two inhalation flow rates (5 L/min and 15 L/min) were used in to represent inhalation under resting and mild exercise conditions in adults.

Sinus ventilation rate

In this study, sinus ventilation rate (q) was calculated to quantify sinus penetration. An artificial surface (S) was imprinted at every sinus ostium to enclose the sinus cavity (Ω). A representative airflow pathline enters the sinus through a surface element at a point and then flows out of the sinus at another point with a surface element. The velocity vector entering the first point is **F**, the surface element normal vector is n, and the angle from n to F is θ. **F** is decomposed into components perpendicular (T) and parallel (II) to **n**. The parallel component of **F** is the airflow proportion that enters the surface element, and the total sinus ventilation is the sum of all surface elements.

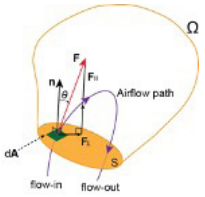

$$q = \frac{1}{2}\int_{S} |\mathbf{F} \cdot d\mathbf{A}|$$

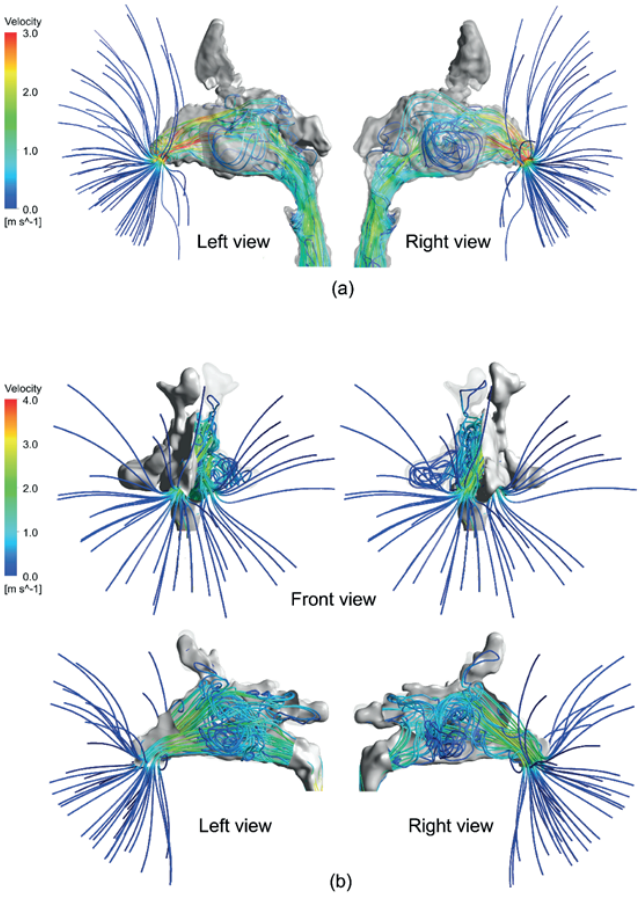

Figure 2. Velocity path streamlines; inhalation flow rate = 15L/min (a) model E (comprehensive FESS) (b) model H (MELP and mega-antrostomy).

Here, **A** is the vector area, which is a combination of the area magnitude of the differential surface element, A, and a unit vector normal to the area **n**, **A** = *A***n**.

Results

Streamlines

Although geometries were different across the models (Figure. 1), general trends in inhalation flow were observed. Figures 2 and 3a display representative findings in Model E (patient 3, comprehensive FESS) and Model H (patient 6, MELP and megaantrostomy). The general inhalation flow was separated into different flow streams that spread out in a superior or inferior direction (Figure 2). Most superiorly, the flow was directed upwards towards the ethmoid sinuses or towards the back of the maxillary sinus and the sphenoid sinus (Figure 2). The remaining flow occurred straight, along the septal wall into the nasopharynx. The degree of air flowing upwards towards the ethmoid sinuses was limited by the size of the internal nasal valve. With a smaller nasal valve, less air entered the ethmoid sinuses and more entered other regions. The most superiorly angled flow stream impinged on the ethmoidal roof and this directed it through the ethmoid sinus toward the sphenoid sinus. All flow that reached the sphenoid sinus had diminished greatly in velocity. Airflow usually entered the maxillary sinus from its posterosuperior aspect, recirculating inside before flowing out inferiorly. Velocity distributions for cross-sections of the internal nasal valve and each of the sinus ostia or sinus cavity openings are displayed for model E (comprehensive FESS) in Figure 3b. Minimal to zero air entered any of the sinuses in both models of limited FESS surgery (models A and C). Negligible flow reached the frontal sinuses in any patient except patient 6 (model H) whom had undergone MELP (Figure 2b). In this patient, major differences were noted due to the absence of part of the septum. Significant flow was directed upwards and medially through the septal window from the right nasal cavity, in the direction of the left ethmoid sinuses. Much less flow crossover occurred from the left to the right nasal cavity, compared to that from the right to the left nasal cavity due to the restriction of flow path by a narrower left internal nasal valve.

Sinus flow partitioning

Results of flow partitioning in the sinuses for each model are displayed in figure 4 as stacked columns displaying airflow distribution between left and right cavities, and different models. Since air was able to recirculate from one sinus to another, and often traversed a sinus region before entering another, the aggregates of inflow from individual sinuses are not aggregates of the total inflow in the sinuses.

Relationship between post-operative geometry and sinus ventilation

The postoperative geometry and sinus flow partition data are included as supplementary material (S1-4 Tables). The correlation between the cross-sectional surface area of each sinus ostia or sinus cavity opening and corresponding sinus ventilation rate is displayed in Figure 5. The trendlines show that a larger sinus ostium correlated with an increase in sinus inflow. This relationship was more accentuated at 15L/min and for the maxillary and sphenoid ostia.

Maxillary ostia

Model A (mini-MMA) had a near-zero maxillary sinus ventilation rate. Models C, E, F, G underwent wide MMA's. The ventilation rate was 11.3-40.5ml/s (4.5-16.2% total airflow) at a flow rate of 15L/min. For models B and D (mega-antrostomies) the ventilation rate was higher – 43.8ml/s-121ml/s (17.5-48.4% total airflow) at a flow rate of 15L/min. Although model H had undergone a MELP with bilateral megaantrostomies, the ventilation rate and percentage of total airflow in the maxillary sinuses were not higher compared to other models who had undergone a standard wide MMA. This was because the distribution of airflow

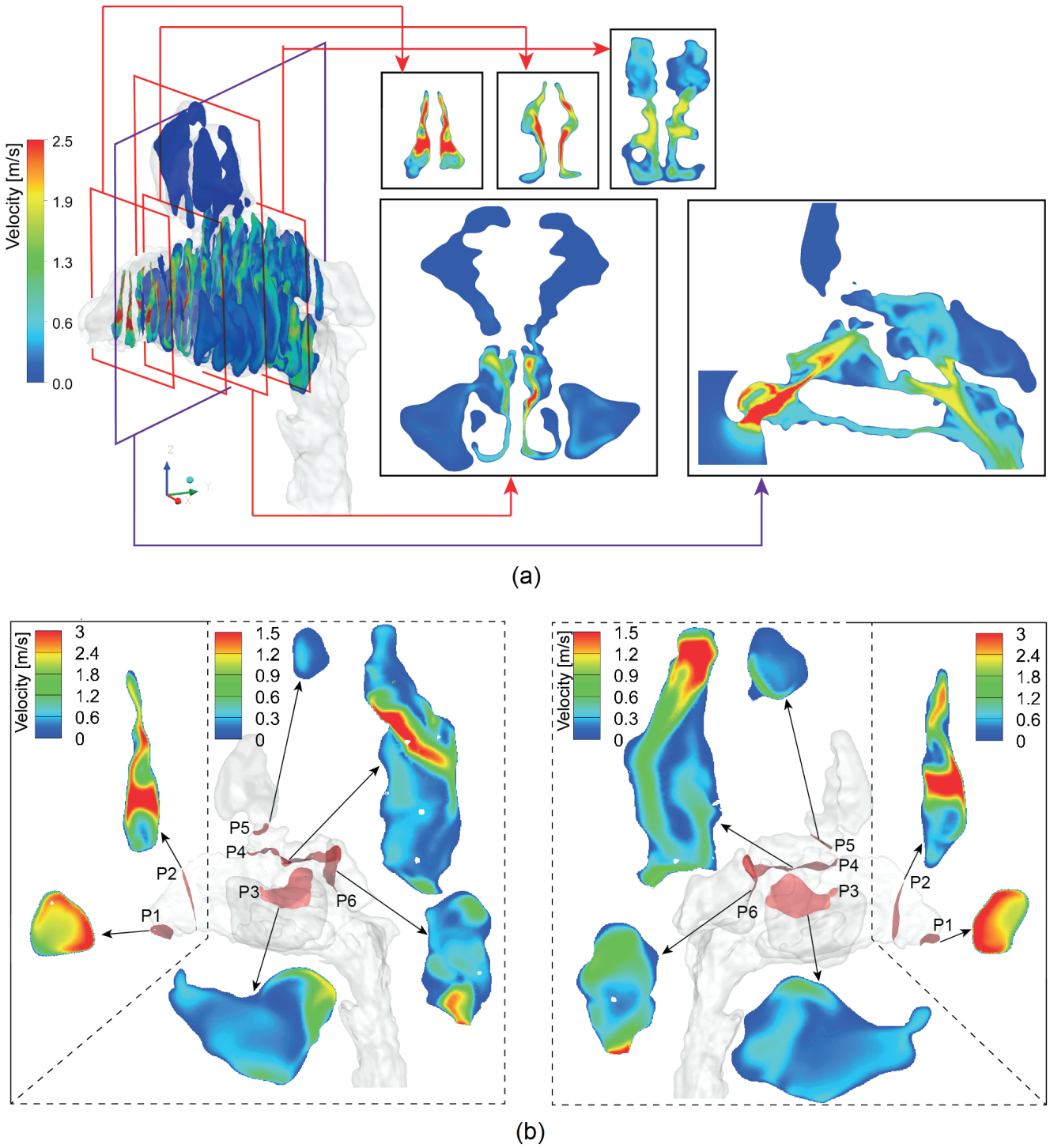

Figure 3. Velocity magnitude contours for model E (comprehensive FESS); inhalation flow rate = 15L/min (a) Velocity distributions in selected coronal and sagittal sections of the nasal cavity in coronal and sagittal planes (b) Velocity distributions at selected openings for model E (comprehensive FESS) displayed from left lateral aspect (pictured left) and from right lateral aspect (picture right); inhalation flow rate = 15L/min. P1 = nostril; P2 = nasal valve; P3 = opening of maxillary sinus; P4 = opening of ethmoid sinus in axial plane; P5 = opening of frontal sinus; P6 = opening of sphenoid sinus.

in the ethmoid sinuses was higher. There was a positive linear correlation between the size of the maxillary antrostomy and maxillary inflow. This was stronger at a flow rate of 15L/min (R2= 0.82) compared to 5L/min (R2= 0.78).

Ethmoid sinus cavity opening

According to the streamline plots, airflow entered the ethmoid sinuses from the main flow stream in an upwards direction. As such, flow partition was studied in the axial plane. For all

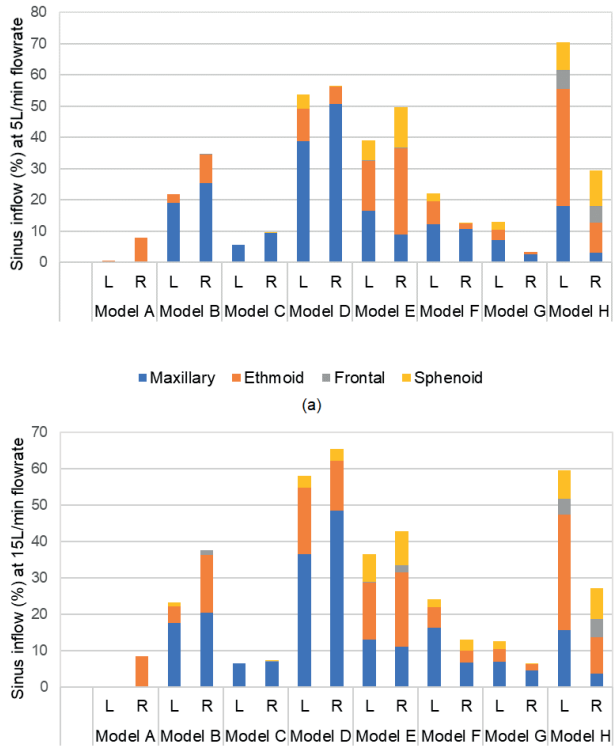

Figure 4. Individual sinus inflow (% of total airflow) (a) inhalation flow rate = 5L/min (b) inhalation flow rate = 15L/min. Since air was able to recirculate from one sinus to another, and air often traversed a sinus region before entering another sinus, the aggregates of inflow from individual sinuses are not aggregates of the total inflow in the sinuses. L = left; R = right.

comprehensive FESS or revision comprehensive FESS models with a complete ethmoidectomy (models B, D, E, F, G), the ventilation rate was 4.3ml/s-51.4ml/s (1.7-20.5% total airflow) at 15L/min. For the MELP model (model H) ventilation in the left ethmoid sinus cavity was up to 79.5ml/s (31.8% total air inflow) at 15L/min flow rate. This was high due to a large amount of air crossover from the right nasal cavity to the left ethmoid sinus cavity through the septal window. Although model G had a comprehensive FESS with total ethmoidectomy, ventilation was as low as 4.3ml/s on the right and 0 ml/s on the left. This variation contributed to an overall weak positive correlation between the area of the opening of the ethmoid sinus cavity and the ventilation rate.

Frontal Ostia

At 5L/min inhalation rate, frontal sinus ventilation was negligible for all models except model H (MELP; 5.1ml/s, right, 4.5ml/s, left), with both frontal sinuses receiving together 11.5% of the total airflow. At 15L/min, ventilation improved for model H (12.3ml/s on the right, 11ml/s on the left). Both frontal sinuses still only received together 9.3% of the total airflow. Frontal sinus ventilation was also improved ipsilaterally to 3.5ml/s for the right frontal sinus in model B and 5ml/s for the right frontal sinus in model E.

Sphenoid Ostia

Models A and C each had unoperated sphenoid sinuses and had negligible ventilation. For models that had undergone wide sphenoidectomy (B, D, E, F, G, H), sphenoid inflow was still minimal at a 5L/min flow rate, except for models E and H (up to 10.8ml/s ventilation rate; 12.9% total air inflow). Models E and H had relatively wider sphenoid ostia (146.7-177.7mm^2). For most models that had undergone wide sphenoidectomy, sphenoid inflow improved at a flow rate of 15L/min. This was especially true for models E and H (up to 23ml/s ventilation rate; 9.2% total air inflow). There was a positive correlation between sphenoid ostium size and ventilation rate at 15L/min (R2= 0.781).

Discussion

This is the largest set of postoperative FESS models used to investigate sinus airflow. The models demonstrated streamline patterns and flow partitioning closely influenced by the type and extent of surgery. In general, streamlines traveled towards the ethmoid sinuses and posterior aspect of the maxillary sinuses at the highest velocity. Whether they entered these regions depended on the extent of surgery in these regions. Frontal sinus ventilation was negligible except in model H (MELP) since it was limited by the narrow frontal ostia and by the path of the main flow stream. Once the air reached the sphenoid sinuses at the back of the nasal cavity its speed had diminished greatly. This meant that entry into the sphenoid sinus tended to be the second lowest (after frontal sinus inflow) across the models. This was slightly higher in one comprehensive FESS patient (model E) and the MELP patient (model H) but for these models, it was still less than 10% for any individual sphenoid sinus.

For patients 1 and 2 who underwent limited surgery (models A and C), total airflow entering the sinuses was low (<10% in model A, <20% in model B). Following revision surgery with a comprehensive FESS and megaantrostomy (models B and D), sinus inflow improved significantly. This occurred particularly in the ethmoid and maxillary sinuses. Close to 50% of the total airflow reached the maxillary sinus on each side in model D and this can be attributed to the much larger size of the antrostomies.

For models E, F and G (comprehensive FESS), airflow occurred mostly in the ethmoid and maxillary sinuses, with maxillary inflow being greater or equal to ethmoid inflow. Although each of these models reflected a similar operation, there was much variability in the amount of airflow in their respective sinuses. The greatest individual sinus inflow in model G reached only 7% (left maxillary sinus) compared to 27.7% in model E (right ethmoid sinus). This shows the varying effect that surgery can have on airflow in any individual. The amount of maxillary inflow overall was comparable to that in a study of maxillary airflow in four FESS patients whom underwent ipsilateral or bilateral FESS

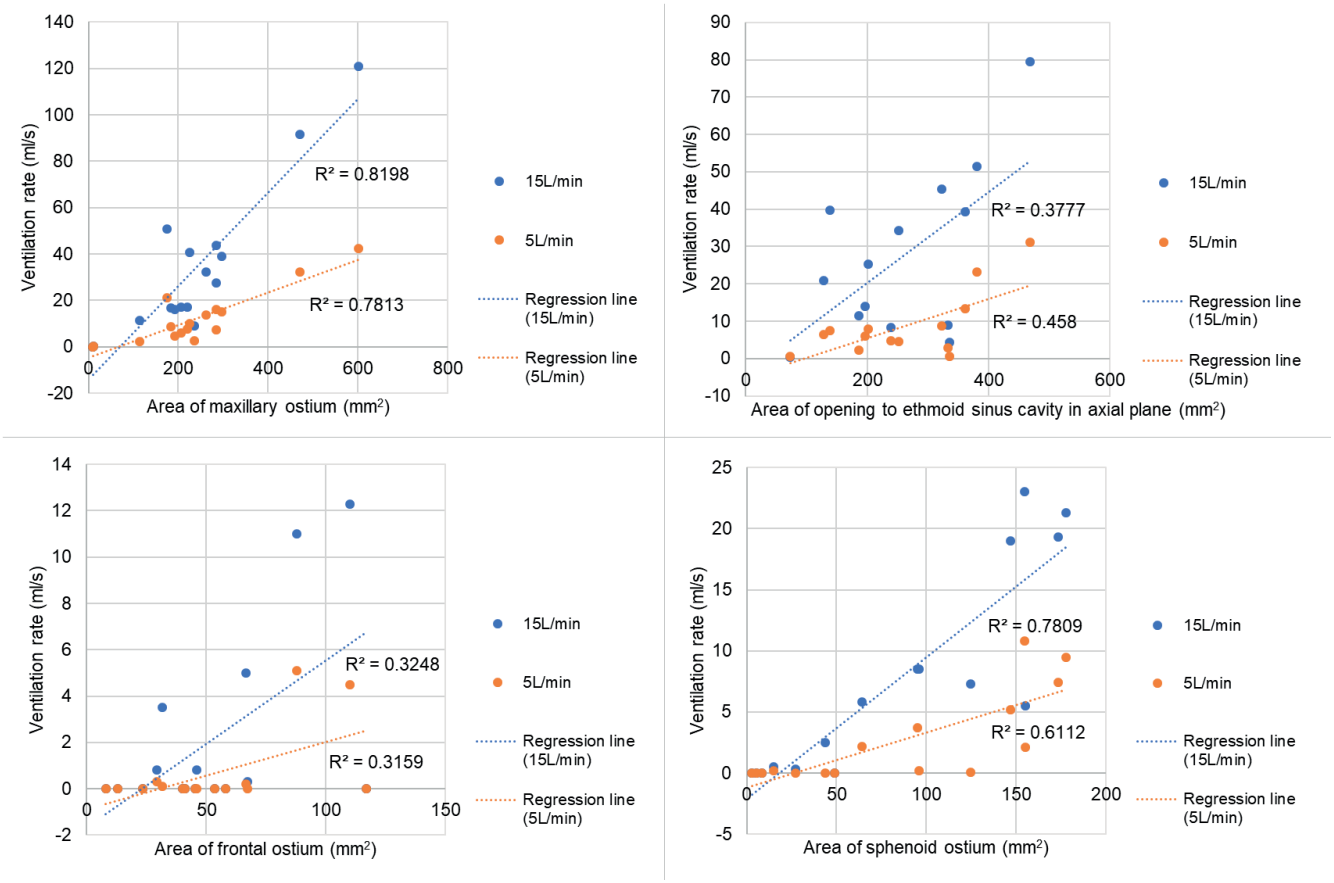

Figure 5. Ostium/sinus cavity opening surface area and sinus ventilation rate at inhalation flow rates of 5L/min and 15L/min.

[3]. In a steady state simulation, they found that both airflow rate and average airflow velocity in the maxillary sinus increased following surgery [3]. These results were supported by another study of maxillary sinus topical drug delivery following FESS.5 Drug delivery was improved in post-FESS models, particularly in those with larger antrostomies [5].

Model H had undergone the most extensive surgery including a MELP and mega-antrostomies. The goal of the MELP procedure is to create a much wider frontal sinus drainage pathway by removing the frontal beak and frontal intersinus septum, in addition to the standard comprehensive FESS. Having a more open sinonasal cavity allowed the highest distribution of airflow into the sinuses compared to other models. Individual frontal sinus airflow reached up to 12.3ml/s (4.9% total airflow) whereas this flow was negligible in all other models. Nevertheless, this is minimal compared to airflow reaching other sinuses. In a study of a single MELP model, although airflow at the frontal sinus ostium was found to be up to four times higher during inspiration, ventilation was still only 8ml/s.10 Airflow entering the sinuses on the left in model H was much greater compared to that on the right, and this is mainly attributed to a large amount of air crossing over from the right nasal cavity to the left nasal cavity through the large septal window. Most of this airflow crossed over into the left ethmoid sinus cavity resulting in high left ethmoid sinus inflow (reaching up to 37.3%). This again demonstrates how surgery and postoperative geometry directly influences airflow.

The correlation between ostia size and ventilation rate was strongest for the maxillary sinuses, a finding consistent with the existing literature [3]. There was also a positive correlation between sphenoid ostium size and sphenoid inflow at an inhalation flow rate 15L/min. All other correlations were weak as an increase in ostium size would often produce very little change in inflow in the related sinus.

Limitations

Preoperative and healthy models were not studied as a baseline comparison since existing literature suggests that sinus inflow prior to surgery is negligible [2-7,10,16,17]. Nasal airflow in healthy models has already been described [4,17,18]. Although this study has relied on the geometry of a small number of patients with surgically treated symptomatic CRS, a broad spectrum of nasal geometry and surgery was represented, from patients having minimal surgery to very extensive surgery with a modified Lothrop procedure and megaantrostomy.

Segmentation and the reconstruction of models suitable

for airflow studies relies on accurate representation of bony cavities. The MR scanning protocol was able to image the entire sinonasal cavity with a high resolution (0.8mm isotropic) [12]. The combination of parameters was sufficient to distinguish the air and soft tissue interface for the segmentation of the sinuses and ostia.

Only inspiratory nasal airflow at a restful steady-state and a breath-hold state was considered in the present study as breathing state is the most common state we experience in daily life, and the respiratory cycle was considered by studying two inspiratory flow rates [19]. Although the effect of the physiological nasal cycle has not been simulated it is expected that there would be some form of alternating partial congestion and decongestion of each nasal chamber occurring. The aerodynamic consequences of this occurring on the mucosa of the turbinates is likely minimal since both inferior and middle turbinates are often reduced to create access for FESS surgery, as was the case for all patients in the study. On the other hand, a narrowing in the internal nasal valve was found to be a significant influencing factor in this study and characterized by a notched appearance in the dorsal anterior nasal cavity in the nasal chamber in some patients (Figure 1). Often this variation in geometry was asymmetrical between two sides, as especially evident in Models A, C, D and H (Figure 1), supporting an alternating cycle. Although further studies would be required to explore the extent of this impact on airflow, variation was considered by including a number of patients and using bilateral airway models.

Conclusion

Following surgery, the nasal cavity and sinuses are more physically and aerodynamically interdependent. This means that an increase in inhalation flow produces an increase in sinus inflow, and conditions leading to an increase in inflow in one sinus will also lead to a reduction in inflow in another. In this manner, FESS greatly enhances sinus aeration. This was particularly evident in the maxillary and ethmoid regions. The extent to which this occurs generally depends on the patient's nasal geometry, such as the internal nasal valve size, or the sinus ostium size which is influenced by the type of surgery. But for unknown reasons, despite having similar surgery sinus inflow may not necessarily improve significantly for all patients. More information is also needed on the effects of FESS on nasal airflow turbulence, drying, heat transfer, and toxic inhalation. A larger cohort of CRS patients is required to validate and broaden the generalizability of our findings.

Acknowledgements

This study was supported by a grant from the Garnett Passe and Rodney Williams Memorial Foundation and funding from AFT Pharmaceuticals.

Authorship contribution

All authors have contributed to data collection, data analysis, and the writing of the manuscript.

Conflict of interest

None

References

1. Zadeh MH, Banthia V, Anand VK, Huang C. Significance of eosinophilia in chronic rhinosinusitis. Am J Rhinol Allergy 2002;16:313-7
2. Chen XB, Lee HP, Chong VF, Wang dY. Aerodynamic characteristics inside the rhino-sinonasal cavity after functional endoscopic sinus surgery. Am J Rhinol Allergy 2011;25:388-92
3. Frank DO, Zanation AM, Dhandha VH, McKinney KA, Fleischman GM, Ebert CSJ, et al. Quantification of airflow into the maxillary sinuses before and after functional endoscopic sinus surgery. Int Forum Allergy Rhinol 2013;3:834-40
4. Wen J, Inthavong K, Tu J, Wang S. Numerical simulations for detailed airflow dynamics in a human nasal cavity. Respir Physiol Neurobiol 2008 161:125-35
5. Wofford MR, Kimbell JS, Frank-Ito DO, Dhandha V, McKinney KA, Fleischman GM, et al. A computational study of functional endoscopic sinus surgery and maxillary sinus drug delivery. Rhinology 2015;53:41-8
6. Zhu JH, Lim KM, Thong KT, Wang dY, Lee HP. Assessment of airflow ventilation in human nasal cavity and maxillary sinus before and after targeted sinonasal surgery: a numerical case study. Respir Physiol Neurobiol 2014;194:29-36
7. Ge QJ, Inthavong K, Tu JY. Local deposition fractions of ultrafine particles in a human nasal-sinus cavity CFD model. Inhal Toxicol 2012;24:492-505
8. Dong J, Tian L, Ahmadi G. Numerical assessment of respiratory airway exposure risks to diesel exhaust particles. Experimental and Computational Multiphase Flow 2019;1:51-9
9. Gu X, Wen J, Wang M, Jian G, Zheng G, Wang S. Numerical investigation of unsteady particle deposition in a realistic human nasal cavity during inhalation. Experimental and Computational Multiphase Flow 2019;1:39-50
10. Kumar H, Jain R, Douglas RG, Tawhai MH. Airflow in the Human Nasal Passage and Sinuses of Chronic Rhinosinusitis Subjects. PLOS ONE 2016;11:e0156379
11. Xiong G, Zhan J, Zuo K, Li J, Rong L, Xu G. Numerical flow simulation in the post-endoscopic sinus surgery nasal cavity. Med Biol Eng Comput 2008;46:1161-7
12. Siu J, Johnston JJ, Pontre B, Inthavong K, Douglas RG. Magnetic resonance imaging evaluation of the distribution of spray and irrigation devices within the sinonasal cavities. International Forum of Allergy & Rhinology 2019;9:958-70
13. Simmen D, Jones N. The Surgical Procedures: safe, logical and Step by Step - Infundibulotomy (Uncinectomy) +/- maxillary Sinusotomy (I, II, III)2014. 139-47 p
14. Shang Y, Inthavong K, Tu J. Detailed microparticle deposition patterns in the human nasal cavity influenced by the breathing zone. Computers & Fluids 2015;114:141-50
15. Inthavong K, Chetty A, Shang Y, Tu J. Examining mesh independence for flow dynamics in the human nasal cavity. Computers in Biology and Medicine 2018;102:40-50
16. Cole P. Nose and sinus airflow. Curr Opin Otolaryngol Head Neck Surg 1994;2:16-21
17. Zhao K, Jiang J. What is normal nasal airflow? A computational study of 22 healthy adults. Int Forum Allergy Rhinol 2014;4:435-

46
18. Tan J, Han D, Wang J, Liu T, Wang T, Zang H, et al. Numerical simulation of normal nasal cavity airflow in Chinese adult: a computational flow dynamics model. Eur Arch Otorhinolaryngol 2012;269:881-9
19. Inthavong K, Tian ZF, Li HF, Tu JY, Yang W, Xue CL, et al. A Numerical Study of Spray Particle Deposition in a Human Nasal Cavity. Aerosol Science and Technology 2006;40:1034-45.

Prof Richard Douglas
Department of Surgery
The University of Auckland
Private Bag 92019
Auckland 1142
New Zealand

Tel: +64 9 923 9820
Fax: +64 9 377 9656
E-mail:
richard.douglas@auckland.ac.nz

This paper contains supplementary materials online: at www.rhinologyjournal.org: https://doi.org/10.4193/Rhin19.387

S1. Table 1. Geometry and flow partition in the maxillary sinus ostium.

Model ID	Surgery	Chamber	Area of maxillary sinus ostium (mm^2)	15 L/min		5 L/min	
					Percentage (%)	Ventilation rate (ml/s)	Percentage (%)
A	Mini-MMA, partial ethmoid.	L	10.1	0	0	0	0
		R	11.5	0.3	0.1	0.1	0.1
B	Rev. comp. FESS, megaantros.	L	284.6	43.8	17.5	15.9	19.1
		R	175.6	50.8	20.3	21.2	25.4
C	Wide MMA, partial ethmoid.	L	192.0	16.0	6.4	4.7	5.7
		R	220.0	17.0	6.8	7.7	9.3
B	Rev. comp. FESS, megaantros.	L	471.1	91.5	36.6	32.2	38.7
		R	601.9	121.0	48.4	42.2	50.7
E	Comp. FESS	L	261.6	32.3	12.9	13.7	16.4
		R	285.6	27.6	11.0	7.4	8.9
F	Comp. FESS	L	225.6	40.5	16.2	10.1	12.1
		R	184.1	16.8	6.7	8.8	10.6
G	Comp. FESS	L	206.1	17.0	6.8	5.8	7.0
		R	113.9	11.3	4.5	2.2	2.6
H	MELP, megaantros.	L	297.0	39.0	15.6	15.1	18.1
		R	235.3	9.0	3.6	2.5	3.0

Mini-MMA = miniature middle meatal antrostomy by partial uncinectomy; partial ethmoid. = partial ethmoidectomy; rev. comp. FESS = revision comprehensive functional endoscopic sinus surgery; megantros. = megaantrostomy; MELP = modified endoscopic Lothrop procedure; L = left; R = right.

S2. Table 2. Geometry and flow partition in the ethmoid sinus cavity in axial plane.

Model ID	Surgery	Chamber	Area of opening to ethmoid sinus in axial plane (mm^2)	15 L/min		5 L/min	
				Ventilation rate (ml/s)	Percentage (%)	Ventilation rate (ml/s)	Percentage (%)
A	Mini-MMA, partial ethmoid.	L	73.3	0.3	0.1	0.5	0.6
		R	127.7	20.8	8.3	6.5	7.8
B	Rev. comp. FESS, megaantros.	L	186.1	11.5	4.6	2.3	2.8
		R	138.8	39.8	15.9	7.6	9.1
C	Wide MMA, partial ethmoid.	L	n/a	n/a	n/a	n/a	n/a
		R	n/a	n/a	n/a	n/a	n/a
B	Rev. comp. FESS, megaantros.	L	323.0	45.3	18.1	8.7	10.4
		R	251.5	34.3	13.7	4.6	5.5
E	Comp. FESS	L	360.9	39.3	15.7	13.4	16.0
		R	380.5	51.4	20.5	23.1	27.7
F	Comp. FESS	L	196.7	14.0	5.6	6.1	7.3
		R	239.4	8.3	3.3	4.8	1.9
G	Comp. FESS	L	332.9	9.0	3.6	2.9	3.5
		R	335.3	4.3	1.7	0.6	0.7
H	MELP, megaantros.	L	467.7	79.5	31.8	31.1	37.3
		R	201.2	25.3	10.1	8.0	9.6

*Not assessed due to majority of ethmoid air cells remaining undissected. Mini-MMA = miniature middle meatal antrostomy by partial uncinectomy; partial ethmoid. = partial ethmoidectomy; rev. comp. FESS = revision comprehensive functional endoscopic sinus surgery; MELP = modified endoscopic Lothrop procedure; L = left; R = right.

S3. Table 3. Geometry and flow partition in the frontal sinus ostium.

Model ID	Surgery	Chamber	Area of frontal sinus ostium (mm²)	15 L/min		5 L/min	
				Ventilation rate (ml/s)	Percentage (%)	Ventilation rate (ml/s)	Percentage (%)
A	Mini-MMA, partial ethmoid.	L	8.1	0	0	0	0
		R	13.0	0	0	0	0
B	Rev. comp. FESS, megaantros.	L	67.1	0.3	0.1	0	0
		R	31.7	3.5	1.4	0.1	0.1
C	Wide MMA, partial ethmoid.	L	40.0	0	0	0	0
		R	46.1	0.8	0.3	0	0
B	Rev. comp. FESS, megaantros.	L	45.4	0	0	0	0
		R	23.4	0	0	0	0
E	Comp. FESS	L	29.2	0.8	0.3	0.3	0.3
		R	66.7	5.0	2.0	0.2	0.2
F	Comp. FESS	L	41.1	0	0	0	0
		R	53.5	0	0	0	0
G	Comp. FESS	L	58.0	0	0	0	0
		R	117.0	0	0	0	0
H	MELP, megaantros.	L	87.7	11.0	4.4	5.1	6.1
		R	109.9	12.3	4.9	4.5	5.4

Mini-MMA = miniature middle meatal antrostomy by partial uncinectomy; partial ethmoid. = partial ethmoidectomy; rev. comp. FESS = revision comprehensive functional endoscopic sinus surgery; MELP = modified endoscopic Lothrop procedure; L = left; R = right.

S4. Table 4. Geometry and flow partition in the sphenoid sinus ostium.

Model ID	Surgery	Chamber	Area of sphenoid sinus ostium (mm²)	15 L/min		5 L/min	
				Ventilation rate (ml/s)	Percentage (%)	Ventilation rate (ml/s)	Percentage (%)
A	Mini-MMA, partial ethmoid.	L	5.5	0	0	0	0
		R	8.2	0	0	0	0
B	Rev. comp. FESS, megaantros.	L	43.5	2.5	1.0	0	0
		R	2.8	0	0	0	0
C	Wide MMA, partial ethmoid.	L	49.1	0	0	0	0
		R	15.0	0.5	0.2	0.2	0.2
B	Rev. comp. FESS, megaantros.	L	95.2	8.5	3.4	3.7	4.5
		R	96.1	8.5	3.4	0.2	0.2
E	Comp. FESS	L	146.7	19.0	7.6	5.2	6.2
		R	154.8	23.0	9.2	10.8	12.9
F	Comp. FESS	L	64.1	5.8	2.3	2.2	2.7
		R	124.8	7.3	2.9	0.1	0.1
G	Comp. FESS	L	155.1	5.5	2.2	2.1	2.5
		R	27.2	0.3	0.1	0	0
H	MELP, megaantros.	L	173.3	19.3	7.7	7.4	8.9
		R	177.7	21.3	8.5	9.5	11.4

Mini-MMA = miniature middle meatal antrostomy by partial uncinectomy; partial ethmoid. = partial ethmoidectomy; rev. comp. FESS = revision comprehensive functional endoscopic sinus surgery; MELP = modified endoscopic Lothrop procedure; L = left; R = right.